Journal of Applied Mathematics and Physics, 2024, 12, 997-1020
https://www.scirp.org/journal/jamp
ISSN Online: 2327-4379
ISSN Print: 2327-4352

Modeling and Simulation of Heterojunction Solar Cell with Mono Crystalline Silicon

Sajid Ullah[1], Ayesha Gulnaz[2], Guangwei Wang[1]

[1]School of Electronic Engineering, Tianjin University of Technology and Education, Tianjin, China
[2]Department of Physics, Rihah International University, Islamabad, Pakistan
Email: sajidullah195@gmail.com, ayeshy.gul285@gmail.com, wgw1632@163.com

How to cite this paper: Ullah, S., Gulnaz, A. and Wang, G.W. (2024) Modeling and Simulation of Heterojunction Solar Cell with Mono Crystalline Silicon. *Journal of Applied Mathematics and Physics*, **12**, 997-1020.
https://doi.org/10.4236/jamp.2024.123061

Received: October 31, 2023
Accepted: March 26, 2024
Published: March 29, 2024

Abstract

The monocrystalline silicon is a promising material that could be used in solar cells that convert light into electricity. Although the cost of ordinary silicon (Si) solar cells has decreased significantly over the past two decades, the conversion efficiency of these cells has remained relatively high. While solar cells have a great potential as a device of renewable energy, the high cost they incur per Watt continues to be a significant barrier to their widespread implementation. As a consequence, it is vital to conduct research into alternate materials that may be used in the construction of solar cells. The heterojunction solar cell (HJSC), which is based on n-type zinc oxide (n-ZnO) and p-type silicon (p-Si), is one of the numerous alternatives of the typical Si single homojunction solar cell. There are many deficiencies that can be found in the published research on n-ZnO/p-Si heterojunction solar cell. Inconsistencies in the stated value of open circuit voltage (V_{oc}) of the solar cell are one example of deficiency. The absence of a full theoretical study to evaluate the potential of the solar cell structure is another deficiency that can be found in these researches. A lower value of experimentally obtained V_{OC} in comparison to the theoretical prediction based on the band-gap between n-ZnO and p-Si. There needs to be more consensus among scientists regarding the optimal conditions for the growth of zinc oxide. Many software's are available for simulating and optimizing the solar cells based on these parameters. For this purpose, in this dissertation, I provide computational results relevant to n-ZnO/p-Si HJSC to overcome deficiencies that have been identified. While modeling and simulating the potential of the solar cell structure with AFORS-HET, it is essential to consider the constraints that exist in the real world. AFORS-HET was explicitly designed to mimic the multilayer solar cell arrangement. In AFORS-HET, we can add up to seven layers for solar cell layout. By using this software, we can figure out the open circuit voltage (V_{OC}), the short circuit current (J_{SC}), the quantum efficiency (QE, %), the heterojunction energy band structure, and the power conversion efficiency (PCE).

Keywords

Heterojunction Solar Cell, Silicon Monocrystalline, Deficiencies, AFORS-HET, Optimization, Open Circuit Voltage, Quantum Efficiency

1. Introduction

The first heterojunction solar cell was probably invented around the year 1983. It has an efficiency of greater than 12%. One kind of photovoltaic cell is known as a heterojunction solar cell. These cells use a p-n junction that combines two distinct semiconductor materials. Compared to conventional single-junction solar cells, using a variety of materials enables the absorption of a greater spectrum of wavelengths, which ultimately results in a better efficiency level. Compared to conventional solar cells, heterojunction solar cells are often more stable and have a longer lifespan. They have found usage in a wide range of applications, such as solar power systems that are located in space as well as solar power systems that are situated on land [1]. A group of researchers at the University of New South Wales in Australia pioneered the development of HIT solar cells, also known as heterojunction with intrinsic thin-layer solar cells, in the late 1990s. By inserting an intrinsic layer of amorphous silicon between the p-type and n-type layers of the solar cell, the team, directed by Dr. Stuart Wenham and Dr. Martin Green, considerably enhanced the efficiency of photovoltaic cells. Which have an intrinsic layer of amorphous silicon that enhances efficiency by absorbing a broader spectrum of wavelengths. HIT solar cells have become industry standards due to their efficiency, stability, and longevity, and are used in both space and ground-based solar power systems. Sanyo's HIT solar cells, which use an ultrathin layer of intrinsic amorphous silicon, have an efficiency of 22.3% and have various applications [2] [3] Thin-film solar cells, which offer scalability and adaptability, were also an area of innovation for Sanyo [4]. The photovoltaic industry, like all others, is motivated by the search for profit. The photovoltaic (PV) industry constantly explores novel production methods to improve solar cells material, and designs to increase device performance and decrease energy costs. SHJ cells, also called silicon heterojunction solar cells, are a promising way to make solar panels that work well and don't cost too much. The outstanding performance of the solar cell is due to its design, which gives it good surface passivation. In this design, the only thing between the bulk and the highly recombinant metal connections is a thin layer of amorphous silicon that acts as a buffer. That's because this particular layer is responsible for all the speed. Consequently, V_{OC} greater than 750 mV are achievable with such a design. SHJ cells are a type of solar cell called a "passivated contact solar cell," a more well-known type. Using silicon with two different morphologies (n-type crystalline silicon for the absorber and amorphous silicon for the p-region) is what gives this junction its "heterojunction" moniker. As a result, the term "heterojunction" was in-

troduced (a-Si). The current world record for silicon solar cell efficiency is 26.7%, [5] recently broken by Kaneka Corporation with a 79 cm^2 solar cell [6]. This is close to the 29% limit for single-junction silicon solar cells [7]. SHJ cells have broken records, but their durability and cost are questioned. Concerns about reliability and cost have led to questions about passivation materials and conductive oxides. Enhancing metallization is a priority. High-temperature pastes cannot be used on standard SHJ. Low-temperature pastes are costly and less conductive. Thin wafers and using SHJ as perovskite bottom cells require better surface passivation for cheaper and more flexible solar cells [8] [9].

The study introduces a multi-scale simulation framework for detailed investigation of transport and device behavior in solar cells, using commercial AFORS-HET tools, highlighting new research on SHJ solar cells. This study focuses on recombination loss and its impact on solar cell performance. It specifically examines n-ITO/n-ZnO/n-In_2O_3/n-Si/i-Si/p-Si/Ag heterojunction solar cells and the role of the n-Si/i-Si passivation layer in carrier movement. The study also discusses the challenges in understanding carrier transport in the unique structure of SHJ solar cells and the need for a comprehensive theoretical framework. The drift-diffusion model is commonly used for simulation studies, but the physics of transport in modern solar cells may deviate from equilibrium. Two key areas of investigation are the high field zone at the n-Si/i-Si/p-Si hetero interface and the carrier transfer through the n-Si/i-Si passivation layer assisted by defects.

2. Simulation Methodology

Simulation of solar cells using software tools like AFORS-Het is crucial for research and improvement of PV technology. AFORS-Het is a program that models heterojunction solar cells and has been effective in advancing solar cell technology. It was developed at Forschungszentrum Jülich in Germany and is based on the drift-diffusion formalism [10]. The program allows for simulating multilayer solar cell setups and calculating various parameters such as power conversion efficiency and quantum efficiency. The AFORS-HET software is commonly used for modeling homojunction and heterojunction devices [11] [12] [13]. It solves one-dimensional semiconductor equations based on partial differential equations (Poisson's equation, continuity equation for holes and electrons) [14], to perform its calculations and uses the Lambert beer law for calculating optical properties. Its expression is given in Equation (1):

$$\frac{\partial \Psi^2}{\partial x^2} = -\frac{\partial E}{\partial x} = -\frac{\rho}{\varepsilon^s} = -\frac{q}{\varepsilon^s}\left[p - n + N_d^+ - N_d^- \pm N_{def}\right] \tag{1}$$

The following expressions describe the carrier continuity:

$$-\frac{\partial j_n}{\partial x} + G - U_n(n,p) = 0 \tag{2}$$

$$-\frac{\partial j_p}{\partial x} + G - U_p(n,p) = 0 \tag{3}$$

The equation relates the hole and electron current density (j_p, j_n) carrier generation rate G, and recombination rates $U_n(n, p)$ and $U_p(n, p)$ in a system. The density of the carrier current is also calculated by:

$$j_p = qn\mu E - qD_p \frac{\partial p}{\partial x} \tag{4}$$

$$j_n = qn\mu E + qD_n \frac{\partial n}{\partial x} \tag{5}$$

In this equation q is the charge, μ_p and μ_n are carrier motilities, and D_p, D_n are the diffusion coefficients [15] [16]. By using these equations, we have calculated the structural components and simulations of a heterojunction solar cell. The cell consists of n-ITO/n-ZnO/n-In_2O_3/n-Si/i-Si/p-Si_3 (gd). het. The goal is to understand the impact of modifying these components on the electrical and optical characteristics and the quantum efficiencies of the cell. The literature-based work functions values of Indium Titanium Oxide (ITO) is 4.4 eV and for Au is 5.1 eV. **Table 1** displays the other material properties that were gathered from the literature for each layer for use in the simulations.

Values for interface defects between ZnO/Si and In_2O_3/Si are shown in **Table 2**, by taking the values from **Table 3** each layer's thickness was tweaked to get the higher possible power conversion efficiency (PCE).

Since there are more negative charge carriers than positive ones, the p-layer must be thicker to make sure that an equal number of positive and negative charge carriers reach the absorption layer. This lets the current density be as high as possible.

Table 1. Material parameters of ZnO, In_2O_3, n-Si, i-Si, p-Si.

Material Parameters	ITO	ZnO	In_2O_3	n-Si	i-Si	p-Si
Thickness (cm)	0.005 (variable)	0.007 -	0.006 -	0.008 -	0.009 -	0.008 -
Energy band-gap (eV)	4.224	3.324	2.724	1.824	1.724	1.12
Electron Affinity	2.05	3.45	4.05	4.05	4.05	4.05
Dielectric Permittivity	7.9	8.9	11.9	11.9	11.9	11.9
CB DOS	2.66E19	3.146E19	2.446E19	2.943E19	2.846E19	2.86E19
VB DOS	1.685E19	1.685E19	1.385E19	1.382E19	1.685E19	1.285E19
Electron/hole thermal velocity	1E6/1E5	1E6/1E5	1E6/1E5	7E6/4E5	1E6/1E5	5E6/4E5
Electron Mobility	1.90E2	7.8E2	5.50E2	1.45E2	1.0E2	1.45E2
Hole Mobility	0.7E2	3.30E2	1.20E2	4.5E2	4.0E2	3.50E2
N_d	3E17	5E17	5E16	7E17	1E9	6E9
N_a	1E9	1E9	1E9	5E8	1E16	6E16

Table 2. Interface defects values of layers.

Material Parameters	ZnO/In_2O_3	In_2O_3/n-Si	n-Si/i-Si	i-Si/p-Si
Defect type	Neutral	Neutral	Neutral	Neutral
Capture cross section for Electrons and holes/(cm^2)	1.0×10^{-14}	1.0×10^{-14}	1.0×10^{-14}	1.0×10^{-14}
Energy distribution Single	Single	Single	Single	Single
E- level w.r.t E_v (above E_v, eV)	0.56124	0.56124	0.56124	0.56124
Total density N_t/cm^3	1.0×10^{14}	1.0×10^{14}	1.0×10^{14}	11.0×10^{14}

Table 3. Arbitrary values of thicknesses of all layers.

Arbitrary Parameters	ITO	ZnO	In_2O_3	n-Si	i-Si	p-Si
Thickness (μm)	0.14	0.0286	0.06	0.01	0.01	0.01

3. Optimization Process

We did an optimization procedure by changing the thickness of one layer while keeping the thicknesses of the other layers the same. The optimal layer thickness was then recorded, along with the highest PCE. Every layer's thickness was adjusted using a different configuration of batch parameters.

The highest PCE was recorded for the layer thickness that had been tuned, which ranged from 20 to 120 μm to kick off the optimization process. The optimized thickness of the ZnO layer was kept, and the thickness of the In_2O_3 layer was changed from10 μm to 110 μm. The PCE was highest at the thickness that matched the layer's optimization. Now, the thickness of the p-Si layer was changed from 40 to 140 μm, while the thickness of the ZnO and In_2O_3-layers stayed the same. The optimum PCE was measured [17] [18]. The n-Si layer's thickness was changed from 30 μm to 130 μm. Our calculations showed that the performance of an n-ITO/n-ZnO/n-In_2O_3/n-Si/i-Si/p-Si_3/Au solar cell device may be improved by optimizing the results against the layer thicknesses. For the best solar cell, researchers looked at how temperature affects the electrical properties and the J-V curve. They also looked at energy band diagrams, quantum efficiency against wavelength, and graphs of carrier production and recombination.

4. Results and Discussion

4.1. Current Density vs Voltage Characteristics of Solar Cell

The input provides a detailed analysis of the current density versus voltage plot (JSC-V plot) for a solar cell under standard illumination conditions. The simulation results in **Figure 1** show the maximum current output of the cell at −20.055 mA/cm^2 when running with no voltage. The graph displays the short-circuit current density (Jsc) at the y-intercepts and the voltage (Voc) at the x-intercepts. A high Jsc value indicates efficient generation of electron-hole pairs in the cell. The Voc is at 0.7947 volts, indicating excellent semiconductor and p-n junction performance with low charge carrier recombination. The fill factor (FF) of

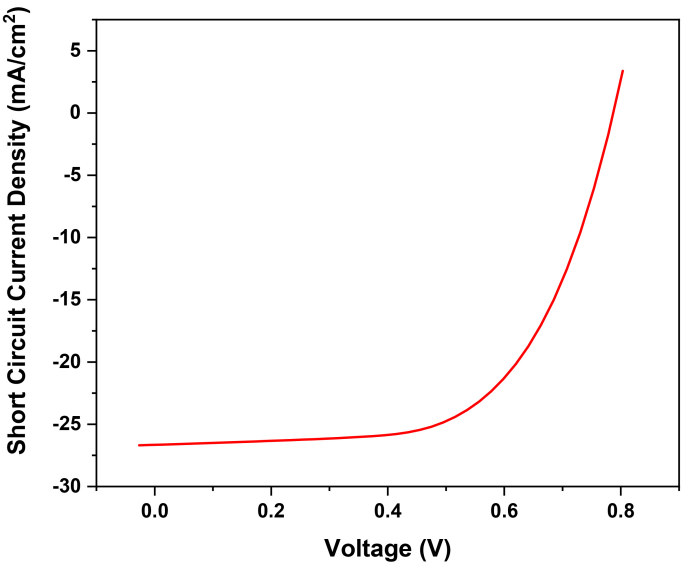

Figure 1. IV curve of solar cell.

61.39% and Power Conversion Efficiency (PCE) of 9.78% demonstrate the cell's reasonable efficiency in converting solar energy into electrical energy. The analysis suggests that minimizing recombination losses could further enhance the cell's performance beyond the current 9.78% efficiency.

4.2. Optimizing Solar Cell Performance by Varying Layer Thickness and Doping Concentrations

4.2.1. Effect of Electron Transport Layer Thickness ZnO

Figure 2 and **Figure 3** explores the impact of ZnO layer thickness (ETL) on device performance. We change the thickness of ZnO from 20 to 120 μm in 20 steps, aiming to achieve comparable output characteristics to the referenced solar cell. The results show that the open circuit voltage (VOC), short circuit current (ISC), fill factor, and power conversion efficiency of the ZnO/Si solar cell increase with increasing/decreasing ZnO thickness. The decrease in short-wavelength photons in the space-charge area and short-circuit current density (JSC) shifts due to the significant difference in doping levels between the materials. As ZnO thickness increases, the number of photons reaching Si contributes most to carrier production. As ZnO thickness grows, the VOC decreases, and the enhanced fill factor is likely due to reduced charge carrier recombination and efficient transport pathways. As the thickness increases beyond this optimal point, physical phenomena may occur, such as increased charge carrier recombination and reduced transport pathways. The device shows a maximum efficiency of 9.79% with a ZnO layer thickness of 20 μm.

4.2.2. Effect of In_2O_3 Layer Thickness (Buffer Layer)

Here, we maintained the previously determined optimal ZnO thickness of 70 μm while varying the In_2O_3 layer thickness (initial solar cell In_2O_3 layer thickness is 60 μm) in 20 discrete increments from 10 μm to 110 μm. **Figure 4** depicts the influ-

ence of In_2O_3 thickness on V_{OC}, J_{SC} and efficiency and fill factor respectively. It was inferred that as the thickness of the In_2O_3 layer increased, the open-circuit voltage and Jsc of the device decreases. The power conversion efficiency (PCE) is considerably increased from 9.78% to 10.57% at In_2O_3 layer thickness of 10 μm. A steep falls off was observed in PCE with the increasing layer thickness. While the photovoltaic device's power conversion efficiency (PCE) exhibits a 1% enhancement compared to the unoptimized solar cell, it is noteworthy that the fill factor experiences a marginal reduction, decreasing from 61.13% to 61.1% (Figure 5).

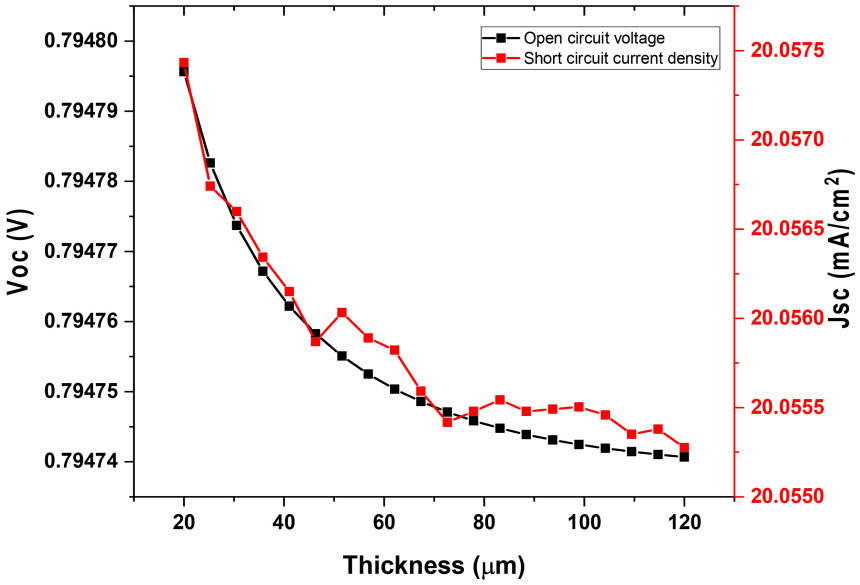

Figure 2. Effect of electron transport layer thickness variation on Voc and Jsc of solar cell.

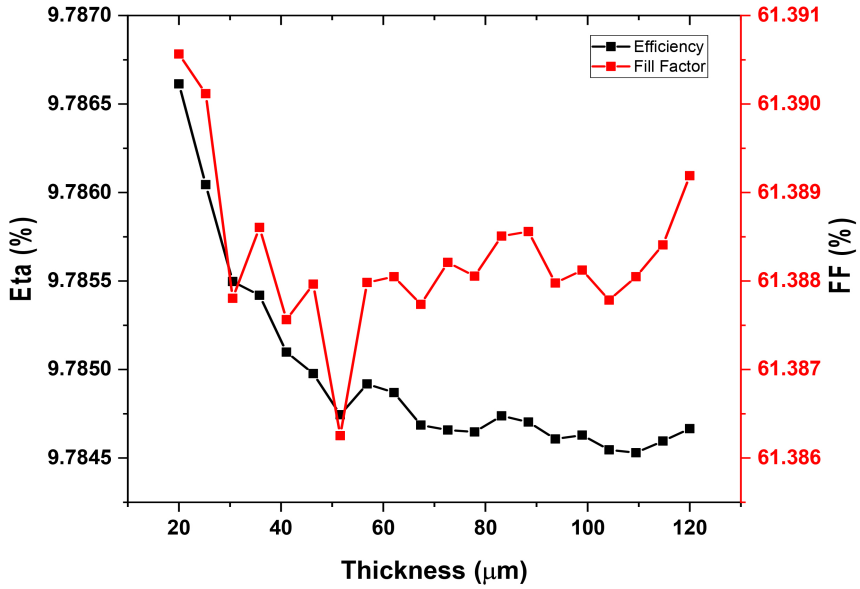

Figure 3. Effect of electron transport layer thickness variation on efficiency and fill factor of solar cell.

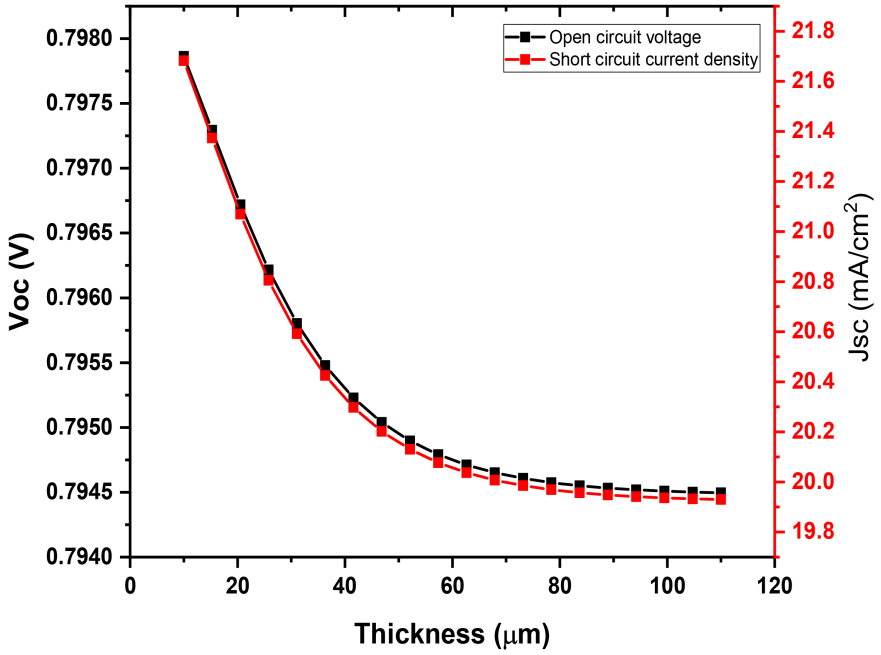

Figure 4. Effect of buffer layer thickness variation on Voc and Jsc of solar cell of solar cell.

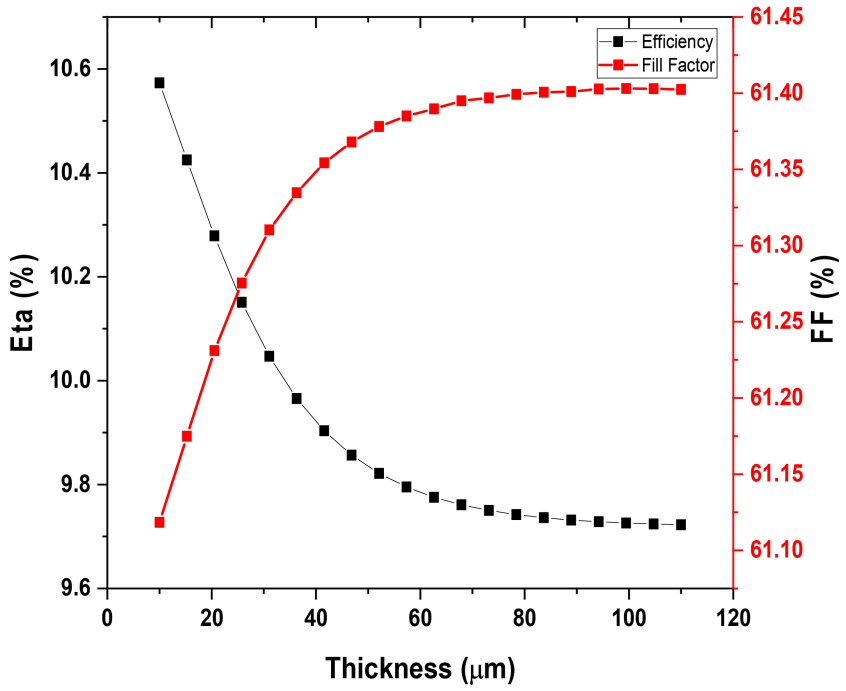

Figure 5. Effect of buffer layer thickness variation on efficiency and fill factor of solar cell.

4.2.3. Effect of n-Si Layer (Absorber Layer)

The thickness of the absorber layer in a silicon solar cell plays a critical role in determining its performance. Optimal thickness is crucial for maximizing light absorption while minimizing carrier recombination. In this step we kept the unoptimized thicknesses of ZnO, and In_2O_3 while we stepped up the thickness of

the Si layer 20 times, from 30 μm to 130 μm. Initially the n-Si layer thickness is 60 μm write Figure 6 and Figure 7 display the effects of varying n-si thicknesses on several electrical characteristics. It was noted that the reduction in absorber layer thickness constitutes a pivotal measure in augmenting the power conversion efficiency (PCE), leading to a substantial increase in overall effectiveness. Decreasing the absorber layer thickness to 30 μm resulted in increase in the efficiency to ~11.5%.

4.2.4. Effect of Intrinsic Si Layer

The intrinsic silicon (Si) layer in a silicon solar cell serves a pivotal role in the device's functionality. Positioned between the P-type (positively doped) and N-type (negatively doped) layers, the intrinsic layer acts as a depletion region, forming a built-in electric field. This field facilitates the separation of photo-generated electron-hole pairs, contributing to the generation of a photocurrent. Additionally, the intrinsic layer helps minimize recombination losses by providing a barrier against the recombination of charge carriers. Therefore, it was important to investigate the intrinsic Si layer thickness role on the overall efficiency and performance of the silicon solar cell. For this purpose we changed the thickness of intrinsic silicon layer (i-Si layer) from 50 to 150 μm (i-Si layer thickness for the initial solar cell is 90 μm) in 20 steps, while keeping other layer parameters to be the same as detailed in section 4.3. The device demonstrated an increase in Jsc, FF and PCE on decreasing the i-Si layer thickness to 50 micron meters, except a slight decrease in VOC as can be observed from Figure 8 and Figure 9.

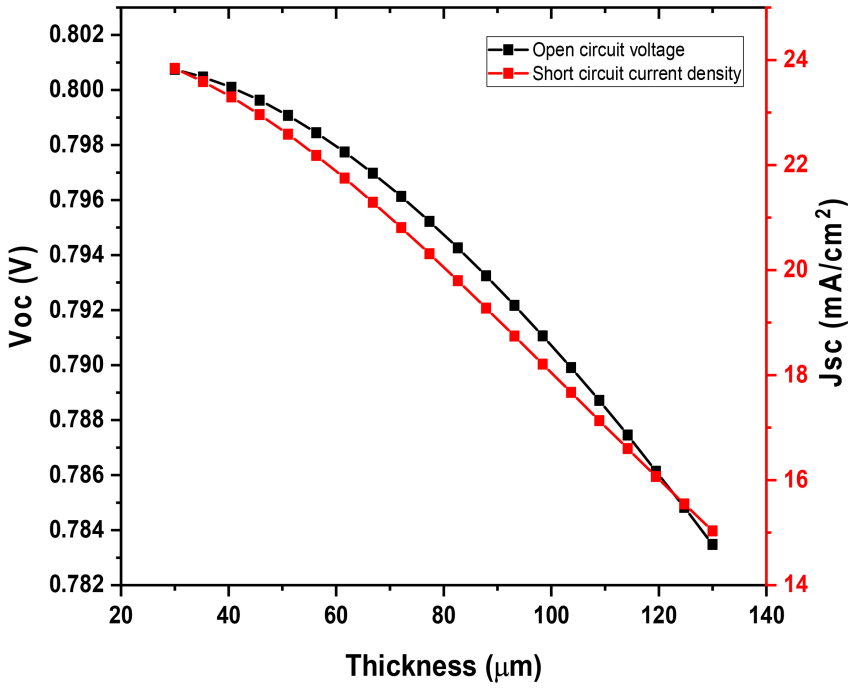

Figure 6. Effect of absorber layer thickness variation on Voc and Jsc of solar cell of solar cell.

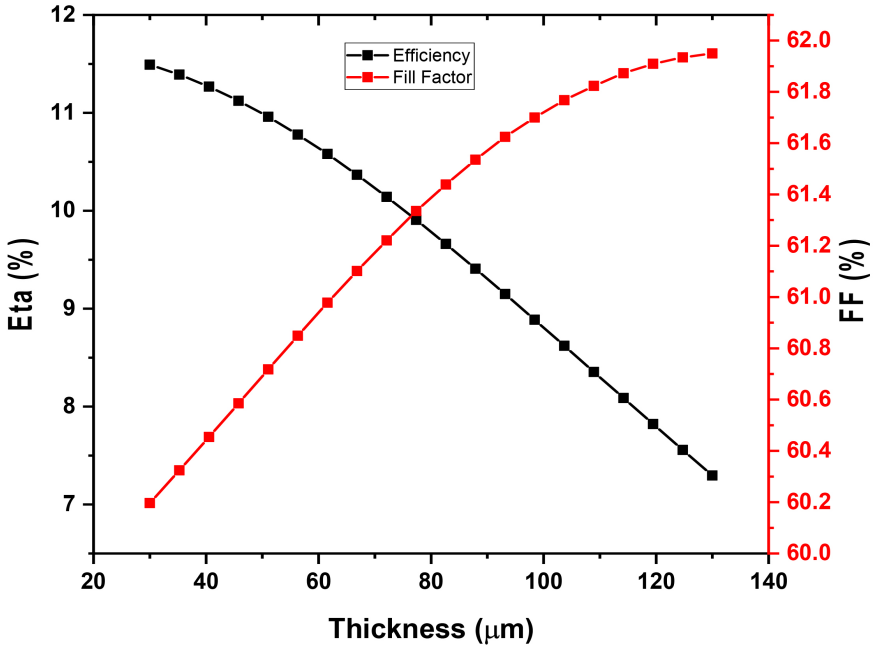

Figure 7. Effect of absorber layer thickness variation on efficiency and fill factor of solar cell.

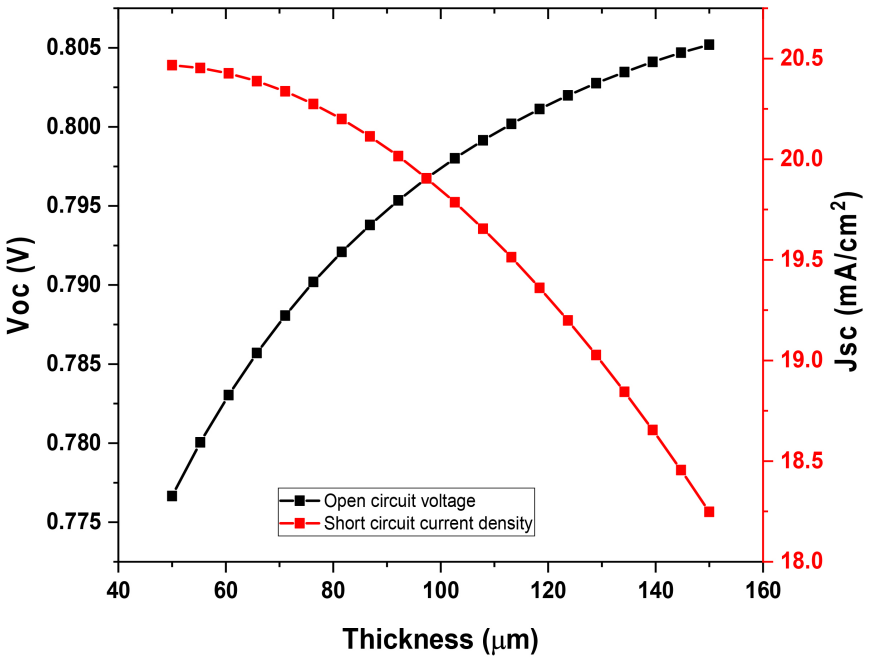

Figure 8. Effect of intrinsic Si layer thickness variation on V_{OC} and J_{SC} of solar cell.

4.2.5. Effect of p-Si Layer Thickness (Hole Transport Layer)

Figure 10 and **Figure 11** depicts the influence of a hole transport layer with a thickness of p-Si on electrical characteristics. In this scenario, the thickness of the p-Si layer is altered from 40 to 140 μm (p-Si layer thickness for the initial solar cell is 80 μm) in 20 discrete steps, while the thickness of the other layers are taken as for the initially simulated solar cell. A marginal improvement was noted

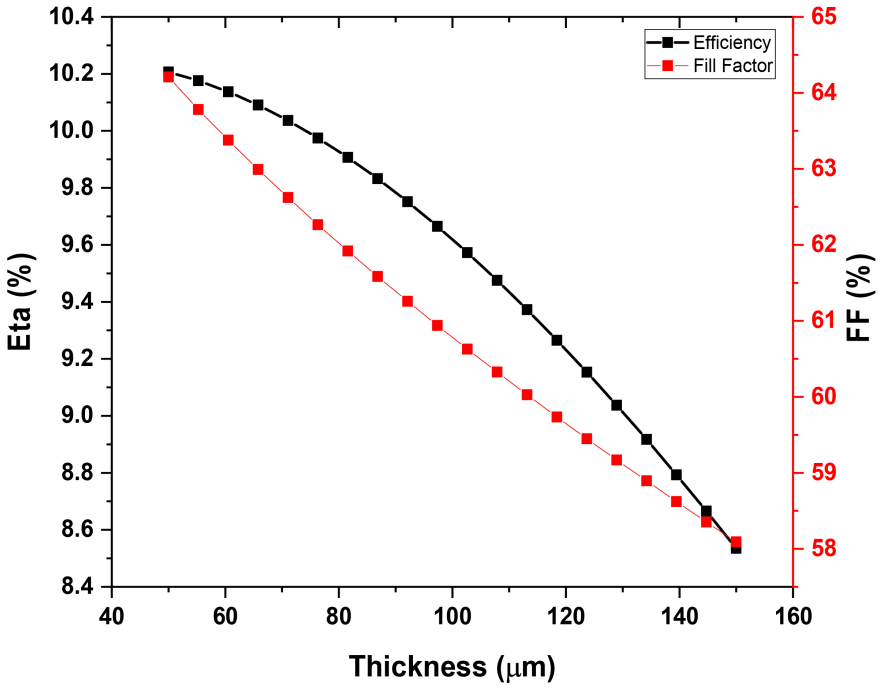

Figure 9. Effect of intrinsic Si layer thickness variation on efficiency and fill factor of solar cell.

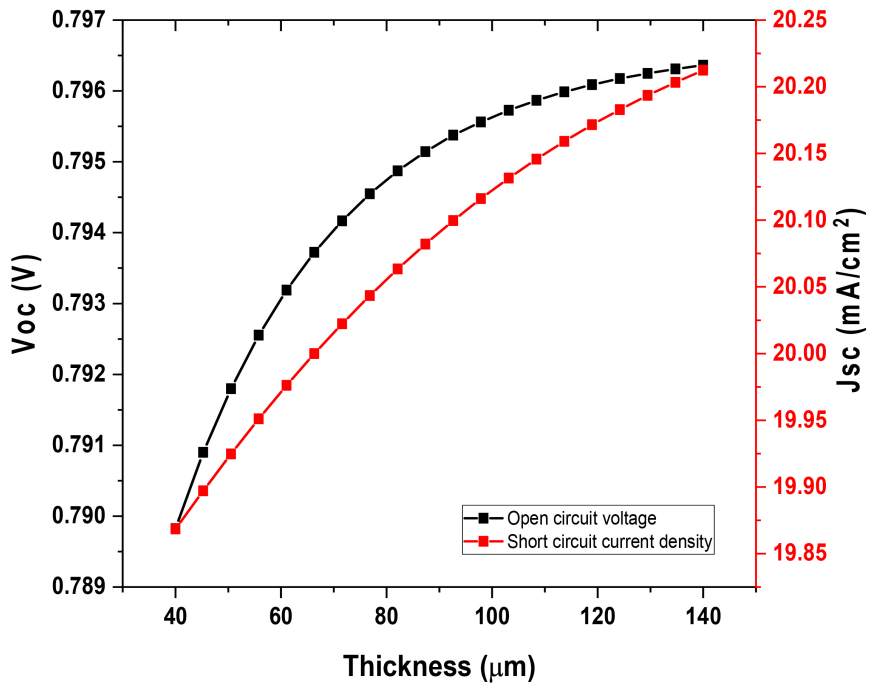

Figure 10. Effect of p-Si layer thickness variation on V_{OC} and J_{SC} of the solar cell.

in the power conversion efficiency (PCE), open-circuit voltage (V_{OC}), and short-circuit current (J_{SC}), with the exception of the fill factor (FF). Nevertheless, there is no discernible alteration in the overall performance of the device compared to the initially selected thickness of the hole transport layer.

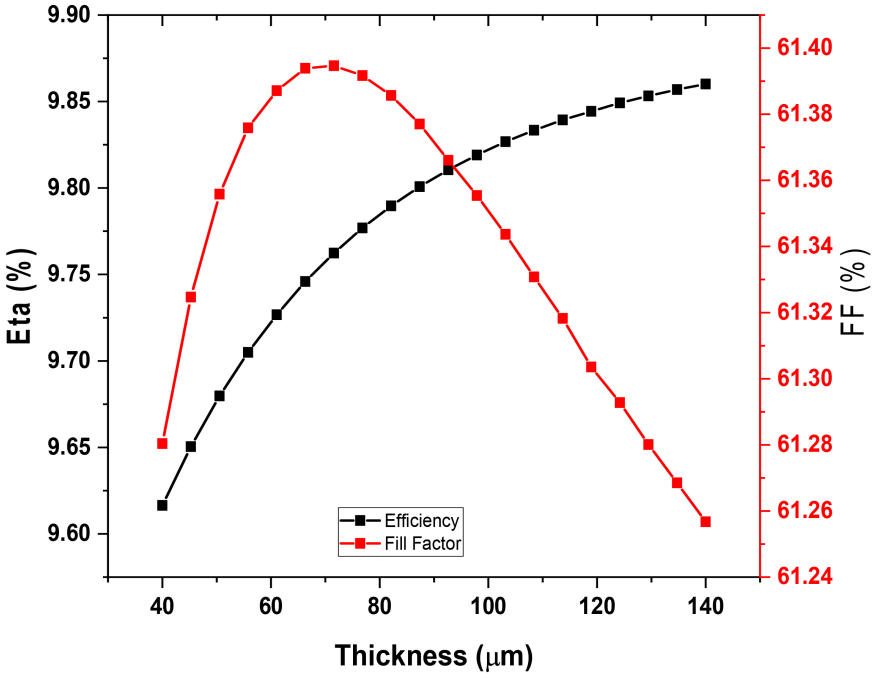

Figure 11. Effect of p-Si layer thickness variation on efficiency and fill factor of solar cell.

4.2.6. Optimized Solar Cell Layer Thickness Parameters

Finally, after these calculations following optimized thicknesses of electron and hole transport layers, absorber and buffer layers' solar cell device was noted:

Optimized thickness of ZnO = 20 μm;

Optimized thickness of In_2O_3 = 10 μm;

Optimized thickness of n-Si = 30 μm;

Optimized thickness of i-Si = 50 μm;

Optimized thickness of pc-Si = 140 μm.

At these optimized thickness values the maximum power conversion efficiency of ITO/ZnO/In_2O_3/si/Au solar cell was observed 12.92%.

4.3. Current Density vs Voltage Characteristics of the Optimized Layer Thickness Solar Cell

The graph in **Figure 12** displays two JSC-V (current density versus voltage) graphs for solar cells under simulated AM1.5G solar spectrum conditions. The graph shows the performance of the optimized and unoptimized solar cells under different voltage conditions. The black curve represents a solar cell that has not been optimized, with a short-circuit current density ranging from 0 to about −30 mA/cm^3. The red curve represents an unoptimized solar cell, with a significant reduction in short-circuit current density.

After optimization, the cell's Voc value is 787.3 mV or 0.7873 V, indicating charge carrier segregation, reduced recombination, and increased open-circuit voltage due to the potential barrier at the p-n junction. The optimized solar cell exhibits a higher Jsc value than the unoptimized cell, indicating that it converts incoming light into electrical current more efficiently across its entire surface

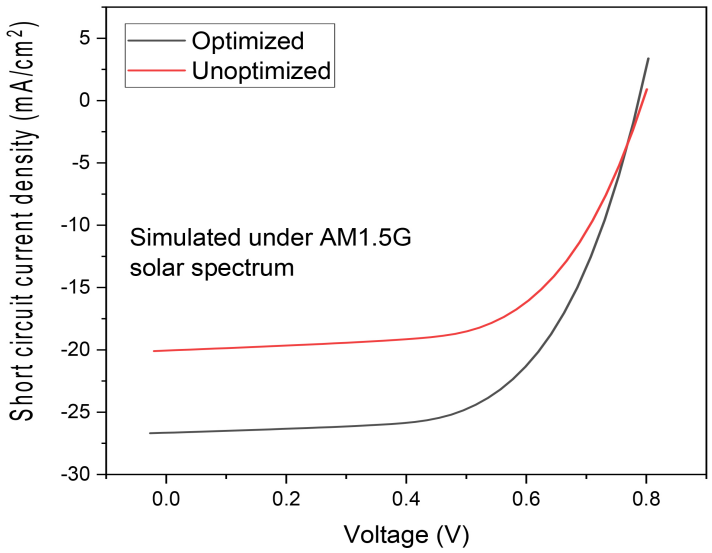

Figure 12. Current density vs voltage plot for the solar cell before layer thickness optimization and the optimized layer thickness.

area. This could be attributed to enhanced light absorption or charge collection efficiency, both of which could result from the optimized thickness of the layer.

The fill factor and maximum Power conversion efficiency for the optimized solar cell are FF = 61.59% and PCE 12.92%, which are higher than the unoptimized solar cell. The optimized solar cell achieved a higher PCE of 12.92% with higher Jsc, similar Voc, and increased FF. This shows that optimizing the layer thickness can significantly influence and enhance the efficiency of solar cells. The black curve's placement on the graph and reduced PCE indicate that the unoptimized cell had lower values for these parameters.

4.3.1. Energy Band Graph of Optimized Solar Cell

The graph in **Figure 13** shows the band alignment and thickness details of an optimized solar cell, with the y-axis representing energy in electron volts and the x-axis representing the position within the solar cell in micrometers. Four energy levels are represented by unique line colors: conduction band edge, valence band boundary, band gap, and Fermi level.

The red lines on the graph depict the conduction band edge, which enhances the material's electrical conductivity and allows electrons to move freely. The almost flat line indicates that the energy of the conduction band remains unchanged, indicating an interface or junction within the cell where the conduction band energy is at its peak. The valence band boundary, denoted by the black line, signifies the energy level at which electrons are present in the states, indicating the presence of a p-n junction or another contact that generates an electric field.

The band gap, which is the distance between the conduction band (Ec) and the valence band (Ev), is a critical component in controlling the cell's efficiency. The graph also shows the Fermi levels for electrons and holes in the n- and

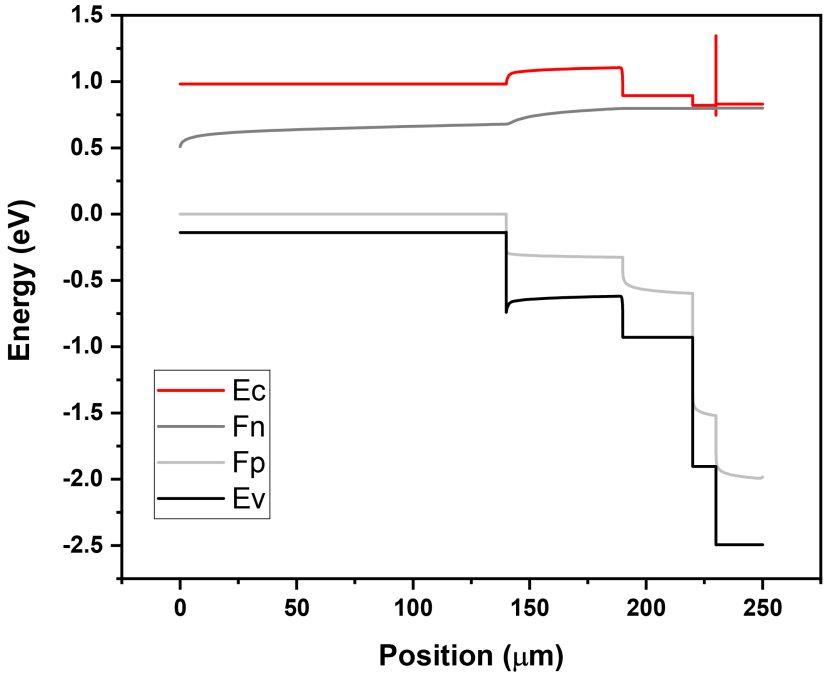

Figure 13. Energy band diagram as a function of position.

p-type, with the Fn and Fp symbols representing the energy levels where the probability of finding an electron and holes is fifty percent.

In conclusion, the fluctuations in Fermi levels suggest the presence of junctions in the solar cell, particularly p-n junctions, crucial for establishing an electric field and segregating charge carriers produced by light absorption.

4.3.2. Recombination Generation Profile

The graph in **Figure 14** shows a fluctuating trend in the generation rate of electron-hole pairs, which involves the creation of pairs. The red line shows a fluctuating trend with several peaks and troughs, indicating variability in generation rate across different locations. The black line shows a more consistent trend overall, remaining steady and not fluctuating as much as the generation rate.

In semiconductor physics, graphs often represent the processes of generation, which involves the creation of electron-hole pairs, and recombination, which involves the annihilation of these pairs. The significant variations in the pattern of the two lines suggest that the techniques or efficiency of formation and recombination processes may vary at various sites inside the material or device under investigation.

Figure 14 illustrates the spatial distribution of electron-hole pair generation and re-combination within the solar cell, offering a detailed view of their dynamics across distinct layers. The total generation rate of electron-hole pairs, amounting to 1E22, signifies the effectiveness of photon absorption and subsequent creation of charge carriers. The recombination rate, recorded at 1E18, sheds light on the processes wherein generated carriers recombine and nullify each other.

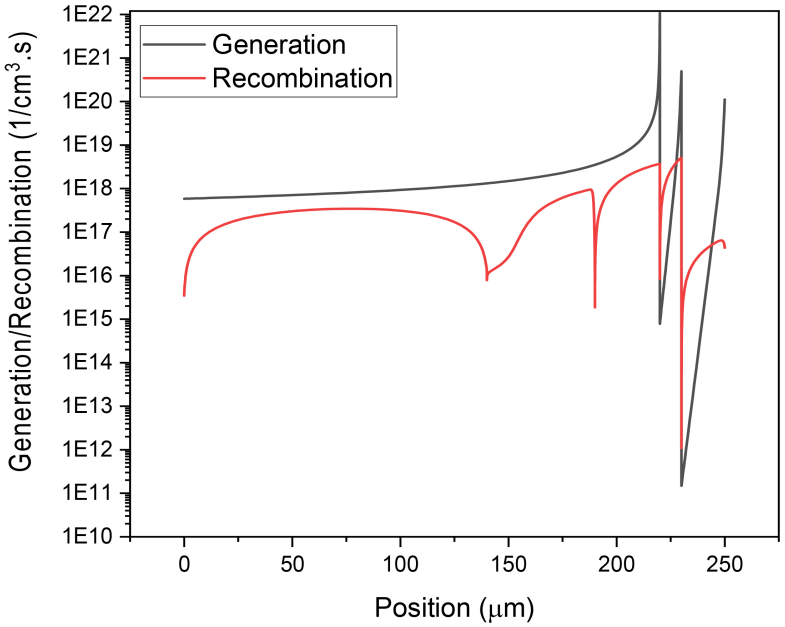

Figure 14. Generation Recombination profile of the solar cell as a function of position.

4.3.3. Carrier Concentration Profile

To gain a more profound insight into the spatial distribution and transport mechanism of carriers within the device, **Figure 15** presents electron (e−) and hole (h+) concentration values along the one-dimensional thickness direction of the solar cell. The figure reveals an observable rise in hole concentration within the electron transport layer and an increase in electron concentration within the hole transport layer. This trend is likely a result of the amplified generation of electrons and holes in the P-N junction under illumination. Initially, as the carriers traverse the absorber layer, the electron concentration surpasses the hole concentration. However, with an increase in thickness, there is a reversal, with the electron concentration becoming lower than the hole concentration. This delineates the identified positions as interfaces, corroborating the presence of the electric field.

4.3.4. Effect of Doping Concentration in Hole Transport Layer (p-Si)

The performance of a silicon solar cell is significantly influenced by the doping concentration in its hole transport layer. Elevated doping concentrations augment carrier mobility, thereby promoting more effective hole transport within the layer. This, in turn, leads to enhanced charge extraction and diminished recombination losses, thereby contributing to an overall improvement in the solar cell's performance. **Figure 16** and **Figure 17** illustrate the influence of varying hole transport layer doping concentration on device performance. It can be observed that efficiency has been surged from 10.5% to 17.2% for varying the acceptor doping concentration from 10E14 cm^{-3} to 10E17 cm^{-3} respectively. Similarly, a significant improvement in other device output parameters can also be observed.

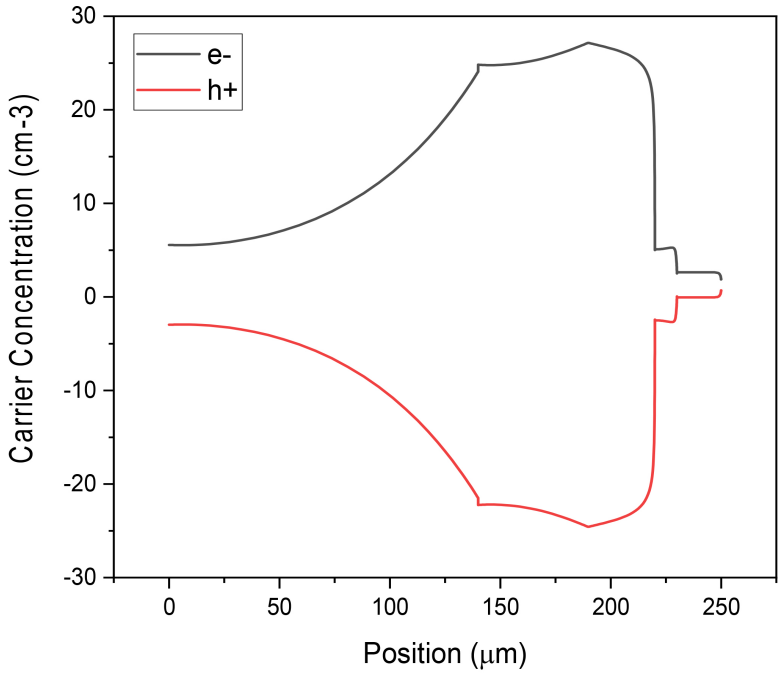

Figure 15. Carrier concentration (electron and hole) profile of the solar cell.

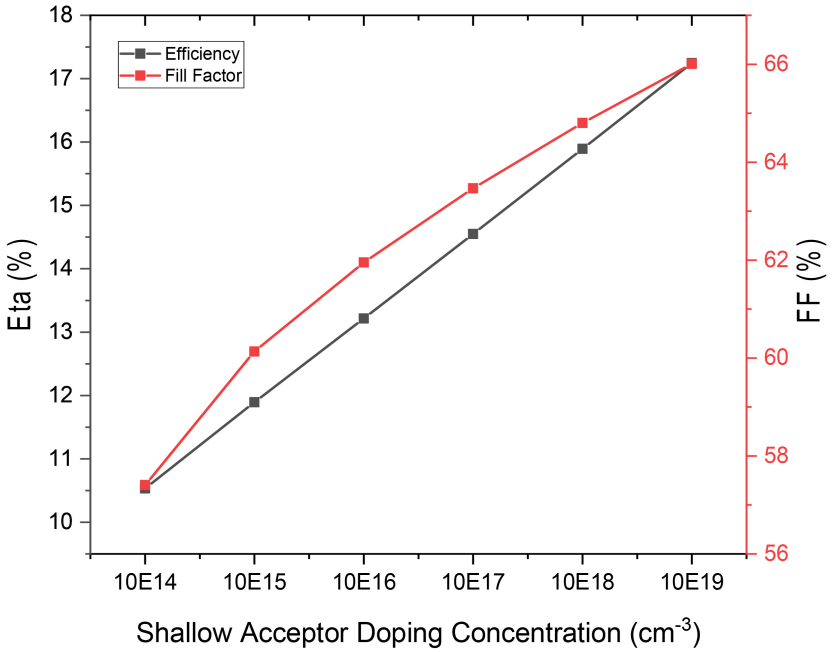

Figure 16. Effect of varying doping concentration on efficiency and fill factor of solar cell.

4.3.5. Effect of Doping Concentration in Buffer Layer (In_2O_3)

The doping concentration within the buffer layer of a silicon solar cell is pivotal in influencing its electrical characteristics. Achieving optimal doping levels in the buffer layer is imperative to establish a favorable energy band alignment between the absorber and adjacent layers. This alignment serves to mitigate carrier recombination at interfaces, thereby augmenting the overall efficiency of the

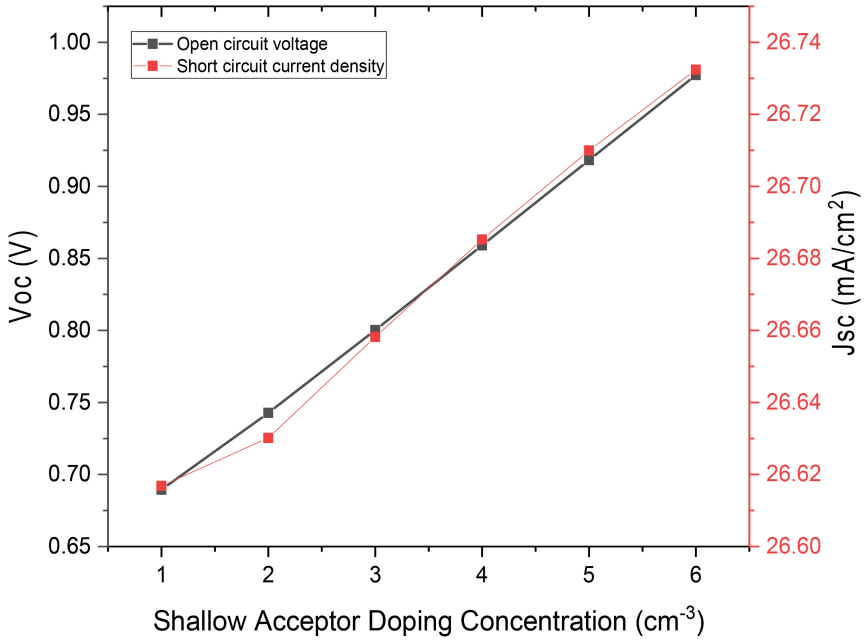

Figure 17. Effect of varying doping concentration on Voc and Jsc of solar cell.

solar cell. **Figure 18** and **Figure 19** depict the impact of varying the doping concentration in the donor transport layer on device performance, ranging from 10E14 cm^{-3} to 10E19 cm^{-3}. Notably, there is only a marginal increase in V_{OC}, from 78.5 mV to 78.7 mV. However, an incremental rise in J_{SC} is observed, escalating from 24.95 mA/cm^2 to 26.4 mA/cm^2 as the donor doping increases from 10E14 cm^{-3} to 10E19 cm^{-3}, respectively. Conversely, there is a substantial enhancement in both device fill factor and efficiency. The fill factor shows a progression from 59.5% to 65.5%, and the efficiency rises from 11.5% to 13.7% across the same range of donor doping concentrations.

It is essential to highlight that the doping concentration in the electron transport layer remains constant, as it has been optimized. Even slight adjustments in the doping concentration, either increase or decrease, may lead to a misalignment in the energy band structure.

4.3.6. External Quantum Efficiency Profile

Figure 20 displays the quantum efficiency of an optimal solar cell based on wave-length, including the visible light spectrum, infrared area, and a portion of the ultraviolet (UV) region. The graph shows that the solar cell has a low external quantum efficiency (EQE) of almost 0% in the ultraviolet region, suggesting it was never intended to convert visible light into usable energy.

In the infrared region, the quantum efficiency increases sharply from 775 nm to 822 nm, reaching a maximum value of 100% at 820 nm. This solar cell is highly suited for converting infrared light into electrical energy, with an EQE value of nearly 1.0%. This peak indicates a limited band of high efficiency compared to regular solar cells, which usually have a larger range of effective wavelengths.

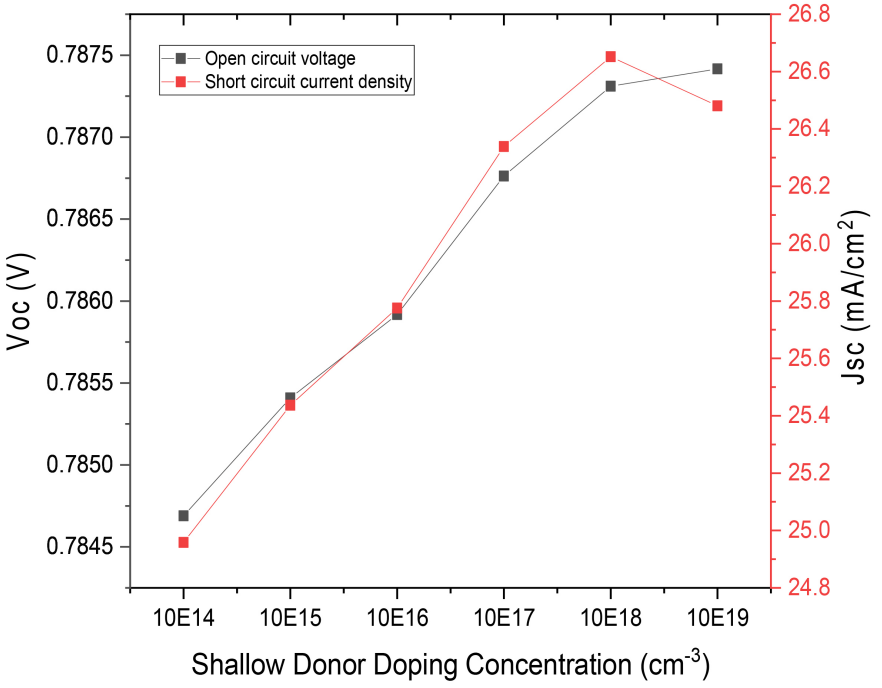

Figure 18. Effect of varying doping concentration on Voc and Jsc of solar cell.

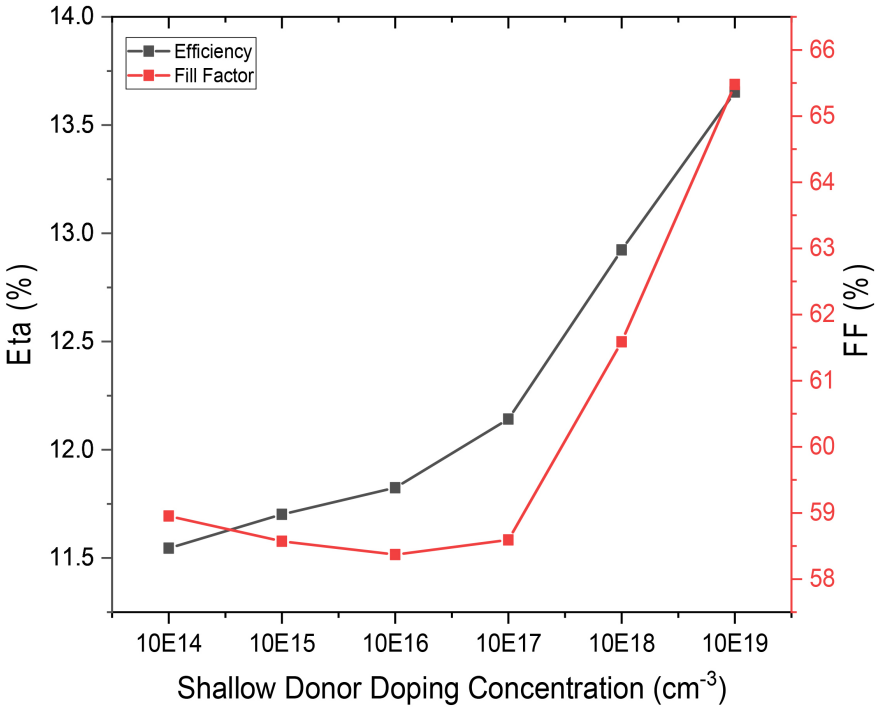

Figure 19. Effect of varying doping concentration on efficiency and fill factor of solar cell.

The solar cell's components include transparent conductive oxide (ITO), zinc oxide (ZnO), indium oxide (In_2O_3), intrinsic silicon (i-Si), n-type silicon (n-Si), p-type silicon (p-Si), and gold (Au). The high EQE in the infrared region is a result of deliberate selection to optimize absorption of infrared light.

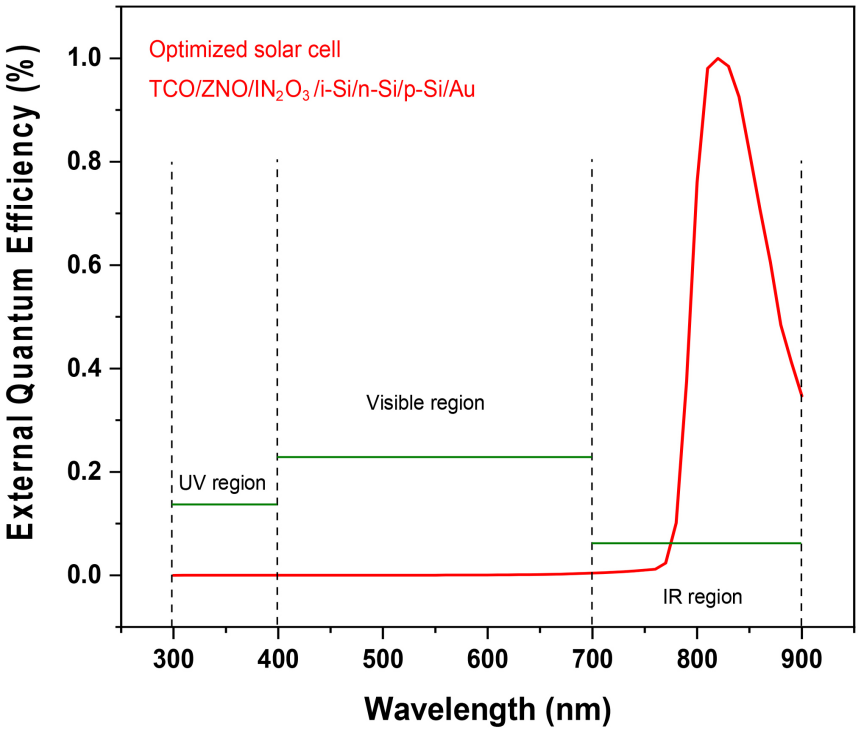

Figure 20. Quantum efficiency of the solar cell.

The graph demonstrates that the solar cell has a narrow and sharp efficiency band, making it best suited for uses where infrared radiation plays a significant role or where a solar cell that doesn't respond to UV or visible light is preferable. It has potential applications in thermal photovoltaics and certain types of sensors. Solar cell technology researchers and engineers would find the released data interesting.

4.3.7. Mott Schottky Analysis

The Mott-Schottky theory, commonly used for p-n junctions, is also applicable to determining the built-in voltage potential in solar cell devices. This evaluation involves utilizing capacitance-voltage (C-V) analysis (refer to **Figure 21**) and Mott-Schottky analysis (refer to **Figure 22**) to gain insights into the electronic properties of the solar cell. The capacitance of a solar cell can provide information on junction quality, defect presence, and charge storage capacity. The C-V analysis in **Figure 21** shows a constant capacitance at around 3 F/cm^2 at −1.0 V, indicating charge storage capability. A slight drop in capacitance around −0.6 V suggests changes within the solar cell, possibly related to charge status or depletion width. The capacitance remains relatively constant between −0.2 V and 0.2 V, indicating maximum charge storage capacity. Beyond 0.2 V, capacitance increases, suggesting higher charge storage with increasing voltage, possibly due to the semiconductor filling traps or states at higher energy levels. A sharp increase in capacitance at 0.8 V may indicate the solar cell nearing its maximum voltage, leading to significant changes in carrier behavior or junction capacitance.

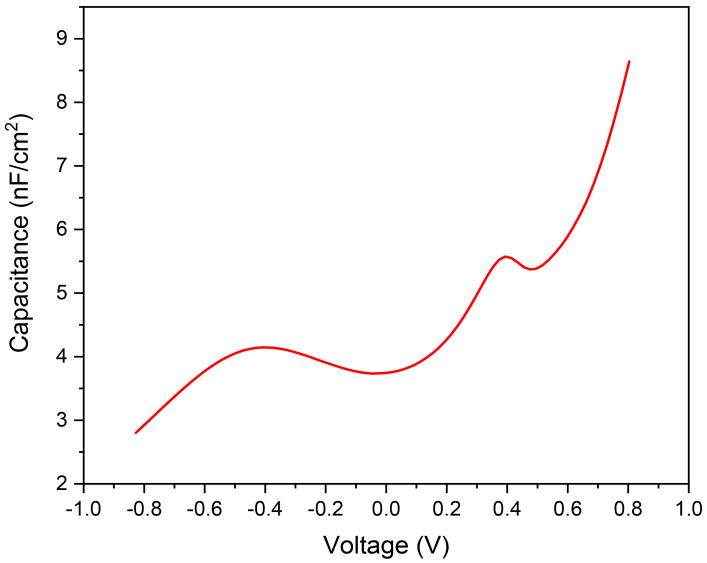

Figure 21. Capacitance vs Voltage profile of the solar cell.

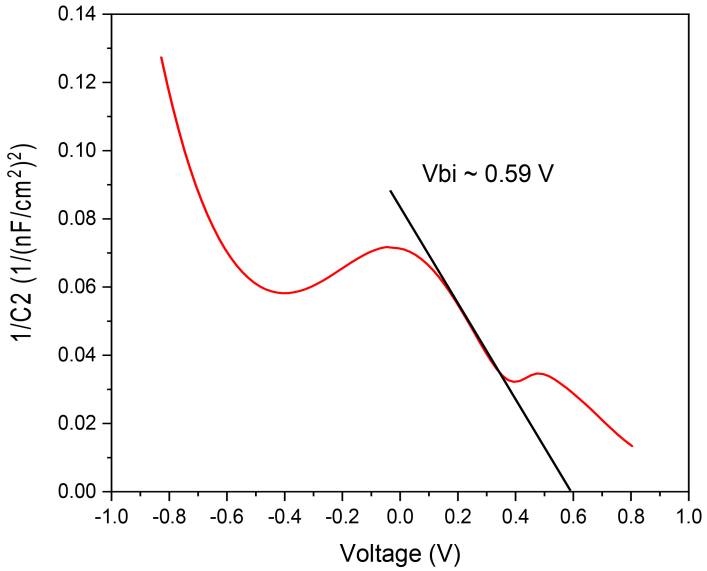

Figure 22. Mott Schottky analysis of the solar cell.

The input describes **Figure 22**, showing a graph depicting scientific data related to a semiconductor diode. The graph illustrates the relationship between voltage and 1/C2 (nF/cm^2), representing the reciprocal of capacitance squared per unit area. The curve on the graph starts at the top left, descends rapidly, reaches a plateau, and then decreases towards the top right. The built-in potential of the solar cell is determined to be 0.59 V, consistent with the open-circuit voltage. The junction of the linear extrapolation of the 1/C2 curve against the voltage curve determines this characteristic value, highlighting the depletion area and built-in voltage of the semiconductor junction. The graph displays two distinct zones: a nonlinear zone on the left and a more linear region on the right, typical of such plots in semiconductor diodes analysis.

4.3.8. Effect of Temperature Variation

In this investigation, we examined the impact of temperature fluctuations on the device performance, spanning a range from 270 K to 350 K to simulate conditions in both cold and extremely hot environments (see Figure 23 and Figure 24). The open-circuit voltage (VOC) experiences a notable reduction from 0.82 V to 0.71 V as the temperature exceeds standard testing conditions. Beyond 300 K, further temperature increases exhibit minimal impact. The fill factor and efficiency exhibit a substantial performance decline at low temperatures, reaching their peak values (64.8% and 13.3%, respectively) at 314 K and 305 K.

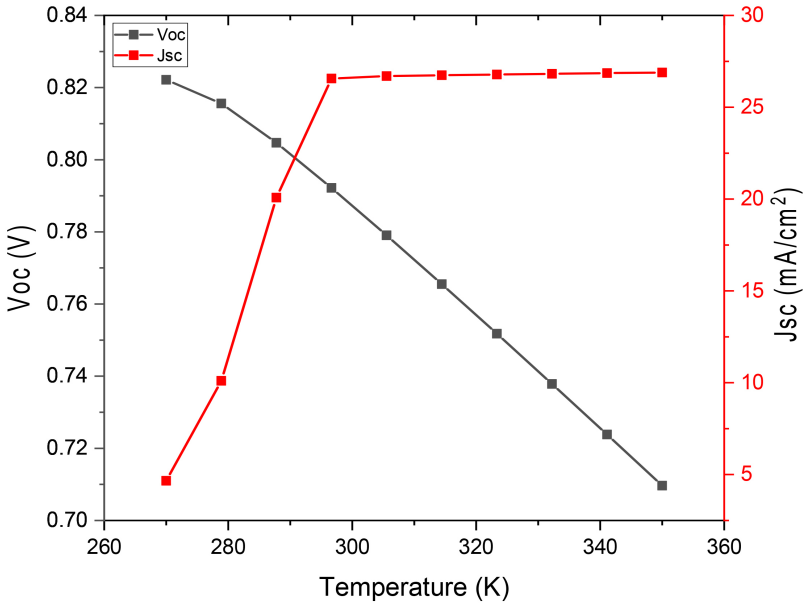

Figure 23. Effect of temperature variation on V_{OC} and J_{SC} of solar cell.

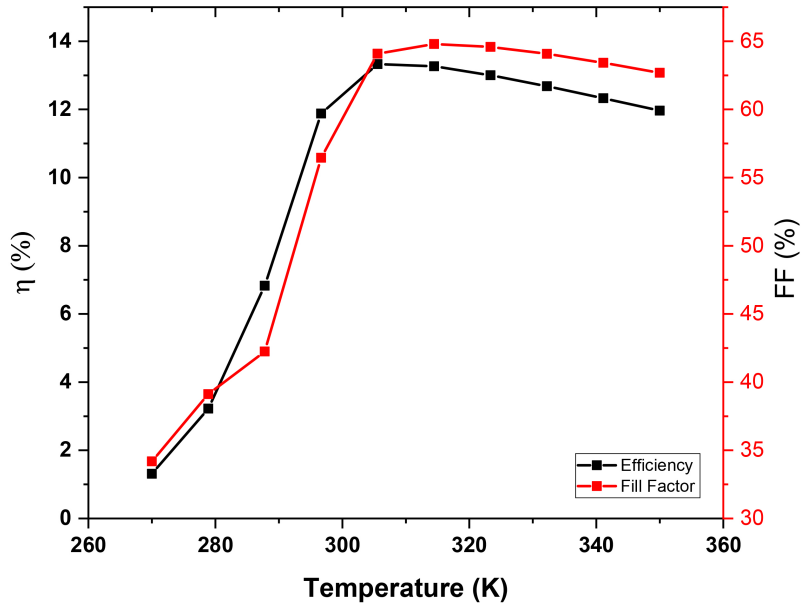

Figure 24. Effect of temperature variation on efficiency and fill factor of solar cell.

5. Conclusions

A comprehensive investigation of the Si-heterojunction solar cell (ITO/ZnO/In_2O_3/n-Si/i-Si/p-Si) has been detailed. It was observed that achieving an optimized device structure is crucial for maximizing performance. The output parameters of the device, namely V_{OC}, J_{SC}, FF, and PCE, exhibited substantial improvements from 794.7 mV, 20.055 mA/cm^2, 61.39%, 9.78% to 787.3 mV, 26.65 mA/cm^2, 61.59%, 12.92%, respectively. The optimization process involved systematically varying the thickness of each layer by approximately ±50 μm around the initially selected thickness, facilitating the identification of the most favorable layer thickness without exhaustive testing.

Furthermore, a comprehensive exploration of the device physics for the optimized structure unveiled improved band alignment, resulting in a decreased electron-hole generation rate relative to the overall generation rate. The study emphasized the significant impact of doping concentration on device efficiency, with an increased p-Si (hole transport layer) doping concentration to 10E19 cm^{-3} leading to a notable enhancement from ~14% to ~17.2%.

Additionally, Mott-Schottky analysis was employed to assess the built-in voltage potential, revealing a value of 0.59 V. The device's resilience to thermal stress at temperatures up to 360 K was demonstrated, with the efficiency being retained over a considerable temperature range. The outcomes underscore the device's promising prospects as a viable contender for the forthcoming production of high-performance Si heterojunction solar cells. The observed results indicate a substantial potential for the advancement and integration of this device into future solar cell technologies, showcasing its suitability for contributing to enhanced efficiency and efficacy in solar energy conversion. The demonstrated performance characteristics position it favorably for further exploration and development in the evolving landscape of solar cell fabrication, emphasizing its potential significance in advancing the frontier of sustainable energy solutions.

Acknowledgements

Special thanks to Dr. WANG GUANGWEI and the School of Electronics Engineering, Tianjin University of Technology and Education, for their invaluable guidance and support.

Conflicts of Interest

The authors declare no conflicts of interest regarding the publication of this paper.

References

[1] Okuda, H.O. and Hamakawa, Y. (1983) Amorphous Si/Polycrystalline Si Stacked Solar Cell Having More Than 12% Conversion Efficiency. *Japanese Journal of Applied Physics*, **22**, L605-L607. https://doi.org/10.1143/JJAP.22.L605

[2] Maruyama, E., *et al.* (2006) Sanyo's Challenges to the Development of High-Efficiency

HIT Solar Cells and the Expansion of HIT Business. 2006 *IEEE 4th World Conference on Photovoltaic Energy Conference*, Waikoloa, 7-12 May 2006, 1455-1460. https://doi.org/10.1109/WCPEC.2006.279743

[3] Hayashi, Y. and Ogura, A. (2013) Role of I-Asi: H Layers in Asi: H/Csi Heterojunction Solar Cells. *IEEE Journal of Photovoltaic*, **3**, 1149-1155. https://doi.org/10.1109/JPHOTOV.2013.2274616

[4] Tanaka, M., Taguchi, M., Matsuyama, T., Sawada, T., Tsuda, S., Nakano, S., Hanafusa, H. and Kuwano Y. (1992) Development of New A-Si/C-Si Heterojunction Solar Cells: ACJ-HIT (Artificially Constructed Junction-Heterojunction with Intrinsic Thin-Layer). *Japanese Journal of Applied Physics*, **31**, 3518-3522. https://doi.org/10.1143/JJAP.31.3518

[5] Limpert, S., *Et Al.*, (2014) Results From Coupled Optical and Electrical Sentaurus TCAD Models of A Gallium Phosphide on Silicon Electron Carrier Selective Contact Solar Cell. *Proceedings of the 40th IEEE Photovoltaic Specialist Conference* (*PVSC*), Denver, 08-13 June 2014, 0836-0840. https://doi.org/10.1109/PVSC.2014.6925045

[6] Green, A., Hishikawa, Y., Warta, W., Dunlop, E.D., Levi, D.H., Hohl-Ebinger, J. and Ho-Baillie, A. (2017) Solar Cell Efficiency Tables (Version 50). *Progress in Photovoltaics*: *Research and Applications*, **25**, 668-676. https://doi.org/10.1002/pip.2909

[7] Shockley, W. and Queisser, H.J. (1961) Detailed Balance Limit of Efficiency of P-N Junction Solar Cells. *Journal of Applied Physics*, **32**, 510-519. https://doi.org/10.1063/1.1736034

[8] Augusto, A., Herasimenka, S.Y., King, R.R., Bowden, S.G. and Honsberg, C. (2017) Analysis of the Recombination Mechanisms of A Silicon Solar Cell with Low Bandgap-Voltage Offset. *Journal of Applied Physics*, **121**, 205704. https://doi.org/10.1063/1.4984071

[9] Herasimenka, S.Y., Dauksher, W.J., Tracy, C.J., Lee, J., Augusto, A., Jain, H., *et al.* (2015). Front- and Rear-Emitter Screen Printed Silicon Heterojunction Solar Cells with >20% Efficiency. In *Proceedings of the 31st European Photovoltaic Solar Energy Conference*, Hamburg, 14-18 September 2015, 761-764.

[10] Conrad, E., Maydell, K.V., Schubert, Ch., Angermann, H. and Schmidt, M. (2006) Optimization of Interface Properties in A-Si:H: H/C-Si Heterojunction Solar Cells. *IEEE World Conference on Photovoltaic Energy Conference*, **2**, 1263-1266. https://www.semanticscholar.org/paper/Optimization-of-Interface-Properties-in-a-Si%3AH-c-Si-Conrad-Maydell/cf05c8cd207dcef7b87bdf3d9974128fa45707e9

[11] Dwivedi, N., Kumar, S., Bisht, A., *et al.* (2013) Simulation Approach for Optimization of Device Structure and Thickness of HIT Solar Cells to Achieve 27% Efficiency. *Sol Energy*, **88**, 31-41. https://doi.org/10.1016/j.solener.2012.11.008

[12] Rawat, A., Sharma, M., Chaudhary, D., *et al.* (2014) Numerical Simulations for High Efficiency HIT Solar Cells Using Microcrystalline Silicon as Emitter and Back Surface Field (BSF) Layers. *Sol Energy*, **110**, 691-703. https://doi.org/10.1016/j.solener.2014.10.004

[13] Dao, V.A., Heo, J., Choi, H., *et al.* (2010) Simulation and Study of the Influence of the Buffer Intrinsic Layer, Back-Surface Field, Densities of Interface Defects, Resistivity of P-Type Silicon Substrate Andtransparent Conductive Oxide on Heterojunction with Intrinsic Thin-Layer (HIT) Solar Cell. *Sol Energy*, **84**, 777-783. https://doi.org/10.1016/j.solener.2010.01.029

[14] Sharma, M., Kumar, S., Dwivedi, N., *et al.* (2013) Optimization of Band Gap, Thickness and Carrier Concentrations for the Development of Efficient Microcrys-

talline Silicon Solar Cells: A Theoretical Approach. *Sol Energy*, **97**, 176-185. https://doi.org/10.1016/j.solener.2013.08.012

[15] Ihalane, E.H., Atourki, L., Kirou, H., Ihlal, A. and Bouabid, K. (2016) Numerical Study of Thin Films CIGS Bilayer Solar Cells Using SCAPS. *Materials Today*: *Proceedings*, **3**, 2570-2577. https://doi.org/10.1016/j.matpr.2016.04.004

[16] MÜLler, J., *et al.* (2004) TCO and Light Trapping in Silicon Thin Film Solar Cells. *Solar Energy*, **77**, 917-930. https://doi.org/10.1016/j.solener.2004.03.015

[17] Wang, D., Wright, M., Elumalai, N.K. and Uddin, A. (2016) Stability of Perovskite Solar Cells. *Solar Energy Materials and Solar Cells*, **147**, 255-275. https://doi.org/10.1016/j.solmat.2015.12.025

[18] Khattak, Y.H., Baig, F., Ullah, S., MarÍ, B., Beg, S. and Ullah, H. (2018) Numerical Modeling Baseline or High Efficiency (Cu 2 Fesns 4) CFTS Based Thin Film Kesterite Solar Cell. *Optik* (*Stuttg*), **164**, 547-555. https://doi.org/10.1016/j.ijleo.2018.03.055